aerospace

MDPI

Article

Dynamic Terminal Airspace Capacity Assessment via Spatio-Temporal Resource–Demand Coupling

Dan Huo *, Di Shen, Fuping Yu, Xiaoyu Zhang and Jixiang Tao

Air Traffic Control and Navigation College, Air Force Engineering University, Xi'an 710051, China; shendi1103@163.com (D.S.); junjingj@163.com (F.Y.); 19567366726@163.com (X.Z.); zhiyuanxingwen@126.com (J.T.)
* Correspondence: kannyh2022@163.com

Abstract

Dynamic terminal airspace capacity assessment remains challenging because operational feasibility is jointly determined by traffic demand and the availability of spatially and temporally heterogeneous airspace resources. This study develops a spatio-temporal resource element (SRE)-based framework that represents physical airspace availability, meteorological conditions, and surveillance support as resource supply, while mapping aircraft trajectories and operational requirements to task demand. A local resource–demand matching mechanism is performed before spatial aggregation to preserve local correspondence and identify resource shortages that may be masked by global indicators. The framework is evaluated using observed ADS-B data from Amsterdam Airport Schiphol, controlled experiments of weather-induced resource degradation, spatial supply–demand mismatch, and traffic-organization variation, together with cross-period robustness tests. An SRE-independent trajectory-based feasibility benchmark is further constructed from complete aircraft-level 4D trajectories using pairwise separation detection and conflict-graph optimization. Under severe weather, the normalized SRE resource-capacity index decreased by 27.8%, while conventional demand-oriented indicators remained unchanged. Under identical global supply–demand conditions, spatial mismatch increased local overload by 15.9%. In the independent trajectory experiment, median feasible throughput increased from 44 to 207 aircraft as candidate demand increased from 50 to 350 aircraft, while the feasible acceptance ratio decreased from 0.88 to 0.59. After controlling for candidate demand, SRE-derived local overload remained positively associated with independently rejected demand, $\rho = 0.452$, $p = 4.9 \times 10^{-19}$. These results indicate that the proposed framework captures both resource-side degradation and localized demand pressure while providing diagnostic information consistent with an independent trajectory-based operational-feasibility benchmark.

Keywords: terminal airspace; dynamic capacity assessment; spatio-temporal resource element; supply–demand matching; air traffic management

Check for updates

Received: 22 August 2026
Revised: 2 October 2026
Accepted: 5 October 2026
Published: 8 October 2026

Copyright: © 2026 by the authors. Licensee MDPI, Basel, Switzerland. This article is an open access article distributed under the terms and conditions of the Creative Commons Attribution (CC BY) license.

1. Introduction

Terminal airspace serves as the transition zone between airport operations and en-route airspace. Affected by converging arrival–departure flows, limited airspace resources, meteorological disturbances and operational constraints, its operations exhibit strong dynamic features. Unlike static capacity estimation, real-world terminal capacity continuously varies with traffic demand and operational-resource availability. Accurate dynamic capacity evaluation and mechanistic interpretation of capacity degradation pose key challenges for modern air traffic management (ATM).

Traditionally, airspace capacity is defined as the maximum number of aircraft safely accommodated under given operational constraints [1]. On this basis, international agencies and researchers have proposed multiple assessment methods for strategic planning and real-time operation [2]. Classical models estimate capacity using throughput, operational limits and airspace layout [3], while terminal-specific models account for arrival–departure flow interactions to quantify capacity limits under diverse scenarios [4]. Optimization-driven techniques have also been proposed to enhance capacity utilization subject to operational constraints [5]. Though effective for capacity planning, these methods adopt an aggregated view and implicitly equate capacity variation with traffic-demand fluctuation. Yet operational capacity is not purely determined by aircraft count. Aircraft consume heterogeneous spatio-temporal resources governed by trajectories, altitudes, separation rules and dwell time; hence identical traffic volumes can produce distinct operational outcomes under different spatio-temporal distributions. To remedy the drawbacks of volume-driven metrics, complexity-based methods were developed to measure traffic-interaction-induced operational burden. Early studies investigated the relationship between air traffic complexity and controller workload, demonstrating that operational difficulty cannot be explained solely by traffic volume [6]. Dynamic density was subsequently introduced to correlate traffic features with controller workload [7]. Follow-up work integrated airspace configuration and traffic interactions to better characterize demand-side pressure [8], and terminal-oriented complexity metrics further incorporated traffic organization and workload factors [9]. These studies confirm that traffic demand alone cannot fully reflect operational difficulty. Nevertheless, complexity-centred approaches focus predominantly on the demand side. They quantify traffic-induced pressure but cannot explicitly measure the reduction in usable operational resources. In practice, capacity may degrade under unchanged traffic demand, since adverse weather, airspace restrictions or surveillance performance loss can curtail available spatial regions and altitude layers [10]. Demand-side indicators cannot distinguish whether capacity loss arises from excessive demand or insufficient resources.

Driven by trajectory-based operations and digital ATM, spatio-temporal modelling has been widely adopted to represent aircraft states. The European ATM Master Plan highlights digitalization and trajectory-based operations for next-generation aviation systems [11], and 4D trajectory simulation tools have been built to capture aircraft movement and operational evolution [12]. Such methods improve the localization of conflicts and constraints by retaining spatio-temporal information, yet most existing implementations only describe aircraft occupancy, lacking an explicit framework connecting airspace resource supply, resource consumption and operational feasibility. Environmental and infrastructure constraints are receiving growing attention in dynamic capacity research. Existing work has verified that convective weather substantially degrades capacity by constraining usable routes and tightening operational limits [13]. However, weather impacts are mostly treated as external disturbances instead of being modelled as modifications to airspace resource states. Accordingly, a refined dynamic capacity framework is needed to explicitly link resource availability and operational demand. It should quantify available resources, resource consumption, and capacity degradation caused by local supply–demand mismatch. Critically, it must preserve spatial correspondence: resource surpluses in one region cannot offset shortages elsewhere under spatial constraints.

To address these challenges, we develop a spatio-temporal resource element (SRE)-based framework for dynamic terminal airspace capacity assessment. Unlike conventional demand-oriented representations, the framework models terminal airspace as a set of spatio-temporal resource elements in which resource availability and operational demand

are represented within the same spatial-temporal reference. The main contributions of this study are summarized as follows:

(1) A spatio-temporal resource representation method is proposed, in which terminal airspace is discretized into resource elements defined by spatial position, altitude layer, and time interval, providing a unified basis for representing dynamic resource states and operational demand.
(2) Multiple influencing factors, including environmental conditions, airspace availability, and surveillance support, are transformed into resource supply, while aircraft trajectories and operational requirements are converted into corresponding task demands, enabling explicit resource–demand coupling.
(3) A local supply–demand matching mechanism is introduced before spatial aggregation to preserve the correspondence between resource availability and operational demand, allowing the identification of localized operational constraints that cannot be revealed by global capacity indicators.
(4) The framework provides a resource-oriented interpretation of dynamic terminal airspace capacity variations by revealing the impacts of resource degradation, spatial resource–demand mismatch, and traffic organization on local operational feasibility.
(5) An SRE-independent trajectory-based operational-feasibility benchmark is introduced using aircraft-level 4D separation analysis and conflict-graph optimization. This benchmark provides an external methodological reference for interpreting SRE-derived local overload without relying on SRE-defined capacity thresholds or resource-accounting quantities.

2. Literature Review

2.1. Conventional Capacity Estimation Methods

Early airspace capacity research focused on the maximum safe traffic volume under given operational constraints. As operations grow more complex, conventional estimation has evolved from static traffic-count metrics toward models incorporating traffic uncertainty, operational constraints and dynamic system properties. Recent work addresses dynamic capacity using stochastic demand, sector configuration and operational variability. Though outperforming deterministic models, these methods mostly treat capacity as an aggregated property for an entire airspace region [14]. Trajectory-driven capacity analysis further integrates aircraft movement features, whereby trajectory information reveals how aircraft distribution and interactions shape operational pressure and capacity, enabling finer terminal airspace description [15]. Optimization-based methods are also widely adopted for demand allocation and capacity utilization, formulating capacity management as constrained optimization to generate feasible traffic solutions under limited airspace resources [16]. Nevertheless, conventional methods focus chiefly on how much traffic airspace can accommodate, rather than why capacity shifts under dynamic conditions. They implicitly attribute capacity degradation to changes in aggregated traffic demand or system loading. Such aggregation overlooks spatial heterogeneity of airspace resources, which may vary independently of traffic due to environmental and operational restrictions.

These approaches commonly assume spatial substitutability of demand: resource shortage in one area can be offset by resources elsewhere, so scenarios with equal total demand are regarded as operationally equivalent. Terminal operations are dominated by local resource availability, since physical layout, weather and surveillance performance vary spatially. Identical aggregated demand may yield distinct operational outcomes when traffic concentrates in resource-limited zones. Hence a capacity description preserving local resource–demand correspondence is required.

2.2. Complexity-Based Capacity Assessment Methods

To overcome limitations of volume-only metrics, traffic-complexity indicators were proposed for evaluating operational difficulty. Dynamic density and related metrics show controller workload depends not only on aircraft number but also on aircraft interactions, spatial distribution and operational characteristics [17]. Subsequent research explored intrinsic airspace complexity affected by traffic structure, aircraft interactions and geometric features, proving complexity is a multidimensional outcome of traffic and operational organization [18]. Workload-oriented studies using multivariate statistics further confirm operational complexity cannot be fully explained by traffic volume alone [19].

Complexity-based methods advance the understanding of demand-side pressure, yet they characterize only how traffic raises operational difficulty. They cannot explicitly quantify available operational resources, nor distinguish whether capacity loss stems from rising demand or resource reduction. Two scenarios with identical traffic complexity may differ greatly in actual operation under divergent weather or airspace availability. Demand-side complexity indicators alone are insufficient to depict dynamic capacity variation.

2.3. Spatio-Temporal Representation Methods in Air Traffic Management

Increasing trajectory data availability promotes spatio-temporal modelling for ATM. Four-dimensional trajectory models describe aircraft movement across space-time and support refined analysis of operational states and traffic interactions [20]. Occupancy-based approaches map aircraft positions into spatio-temporal cells to detect local congestion and capacity constraints invisible to global indicators [21]. Recently, graph-based and data-driven methods have captured spatio-temporal dependencies to better characterize traffic evolution and conflict propagation [22]. However, existing spatio-temporal frameworks focus mainly on where and when aircraft operate, rather than quantifying available resources at given space-time locations. Occupancy- and trajectory-based approaches usually infer airspace state from aircraft presence, implicitly equating unoccupied areas with usable capacity.

This assumption fails under dynamic operations. A region free of aircraft is not guaranteed to have surplus resources; it may become unavailable due to adverse weather, airspace restrictions or surveillance degradation. Lacking explicit resource-side descriptions, current models cannot differentiate real capacity availability from resource unavailability. A complete dynamic capacity representation must jointly capture spatio-temporal resource supply and operational demand, so that capacity-degradation mechanisms hidden in pure trajectory-occupancy analysis can be identified.

2.4. Demand–Capacity Balancing and Optimization Approaches

Besides capacity estimation and state representation, demand–capacity balancing (DCB) is a key ATM research stream. DCB is generally formulated as an optimization problem that adjusts traffic demand to match capacity limits. Traditional optimization relies on mathematical programming and heuristics for traffic regulation and congestion mitigation [23]. With advances in intelligent optimization, learning-based techniques have been introduced for DCB. Reinforcement learning generates adaptive traffic-control strategies for complex operational environments for dynamic capacity management [24]. Multi-agent reinforcement learning improves scalability by treating flights or sectors as interactive agents, and deep reinforcement learning solves large-scale DCB under intricate flight-level constraints [25]. Image- and graph-oriented deep learning further enhance complex-traffic-state representation and DCB decision performance.

Despite these achievements, most optimization- and learning-based approaches treat capacity as an externally given constraint instead of explicitly modelling resource evolution

driven by the environment and operations. Accordingly, DCB performance hinges heavily on the accuracy of capacity input. Mechanism-driven resource-demand representation is therefore needed to supply spatially explicit dynamic capacity information for future capacity management.

3. Methodology

This methodology uses the spatio-temporal resource element (SRE) as a common spatial-temporal unit to represent resource supply and task demand in terminal airspace. Airspace structure, meteorological conditions, and surveillance support are mapped onto the SRE scale to determine potential resource supply through minimum-feasibility gating and continuous supply-quality weighting, while aircraft trajectories and operational protection envelopes are mapped onto the same scale to characterize task resource demand. The feasibility gate only determines whether an SRE can form effective resource supply and does not constitute an independent capacity layer. Supply and demand are first matched locally at the SRE level to obtain residual resources and local overload, and are then aggregated across spatial regions, altitude layers, and time windows. This local-matching-first procedure preserves their spatio-temporal correspondence and prevents resource surpluses at other locations from concealing local shortages.

3.1. Definition of SRE

An SRE is defined as the fundamental spatio-temporal unit for organizing resource states, mapping task occupancy, and performing resource accounting in complex terminal airspace:

$$SRE_i(t_m) = \langle g_i, I_m \rangle \tag{1}$$

$$I_m = [t_m, t_{m+1}],\ m = 1, 2, \ldots, N_t \tag{2}$$

Here, g_i denotes the ith spatial grid voxel and I_m denotes the mth time interval. The spatio-temporal identity of an SRE is determined solely by its spatial grid and time interval and is therefore independent of a specific operational scenario. Different scenarios alter the supply attributes, task demand, and residual resource state associated with the same SRE, but do not alter its underlying spatio-temporal definition.

Let the study airspace be represented by the three-dimensional domain Ω, with the spatial grid set as $G = \{g_i | i = 1, 2, \ldots, N\}$ and the set of discrete time intervals given by Equation (2). The set of resource elements within the study domain is then expressed as

$$S = \{SRE_i(t_m) = \langle g_i, I_m \rangle \mid g_i \cap \Omega \neq \emptyset\} \tag{3}$$

For grid cells intersecting the boundary of the study domain, the geometric fraction lying within the domain is defined as

$$u_i^{\Omega} = \left| \frac{|g_i \cap \Omega|}{|g_i|} \right| \tag{4}$$

where $u_i^{\Omega} \in [0, 1]$ and $|\cdot|$ denotes three-dimensional spatial volume. The quantity u_i^{Ω} represents only the geometric mask associated with the boundary of the study domain and is independent of physical availability losses caused by restricted areas or obstacles. Before entering the model, multi-source data describing airspace structure, meteorological conditions, surveillance coverage, and trajectories are aligned to the common (i,m) index through spatial overlap, interpolation or coverage mapping, and temporal synchronization. A common horizontal grid resolution, vertical layer thickness, and time step are used across

the study and all primary comparison scenarios so that different scenarios can be evaluated on the same spatio-temporal basis.

Local resource supply, task demand, residual resources, and overload are all quantified in SRE-equivalents (SRE-eq). Under a given discretization configuration, an SRE that lies entirely within the study domain, passes the resource-feasibility criterion, and attains the reference upper level for all supply attributes is assigned a nominal supply of 1 SRE-eq. For a boundary SRE, the maximum nominal supply is u_i^{Ω} SRE-eq.

SRE-eq should not be interpreted directly as either the number of aircraft movements or a purely geometric volume. Rather, it is a normalized resource-accounting unit defined relative to an intact and fully available reference SRE under a specified spatial grid and time step. SRE-eq itself is therefore not equivalent to terminal airspace capacity. Instead, it serves as the elementary accounting unit from which the proposed SRE-based resource-capacity representation is subsequently constructed through aggregation of effective resource supply. Consequently, absolute SRE-eq values depend on spatial and temporal resolutions and should only be compared across scenarios using the same discretization settings. The conceptual representation of spatio-temporal resource elements and multi-source resource mapping is illustrated in Figure 1.

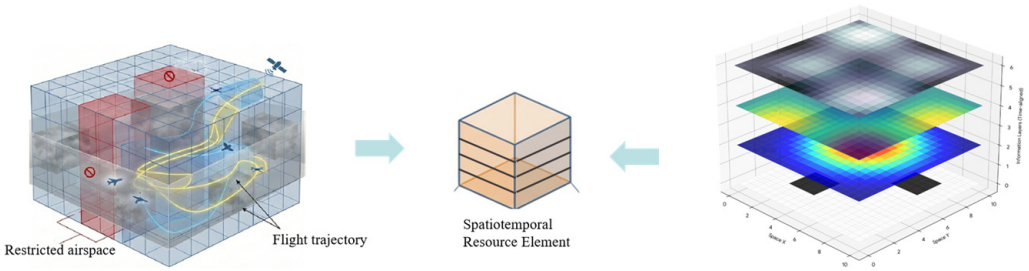


Figure 1. Conceptual representation of spatio-temporal resource elements and multi-source resource mapping. Different layers represent distinct attribute layers, and the color within each layer indicates the corresponding attribute values.

The framework assumes a consistent spatial-temporal discretization within each comparison set, quasi-steady supply conditions within each time interval, additivity across non-overlapping SREs, an exogenously specified task set, and local non-substitutability of resources under fixed trajectories and operating times. Rerouting, delay, altitude adjustment, and conflict-resolution actions are therefore outside the present resource-side accounting framework.

3.2. Resource Supply Estimation

Based on the SRE definition, potential resource supply represents the amount of effective resources that can be formed by each resource element under a given operating environment. Resource supply is characterized in three dimensions: physical availability, meteorological availability, and surveillance coverage. A two-stage structure consisting of minimum-feasibility gating followed by continuous supply-quality weighting is used to determine the potential resource supply of each SRE.

3.2.1. Resource Supply Attributes

For any resource element $SRE_{i,m}$, its potential resource supply is determined by the supply-side operating conditions associated with that spatio-temporal location.

(1) Physical availability, denoted by $\mu_i(t_m)$, characterizes the effects of airspace structure and spatial constraints on the availability of a resource element. Let $\mathbf{g}_i^{\Omega} = \mathbf{g}_i \cap \Omega$ denote the effective portion of grid cell $\mathbf{g}_i$ lying within the study domain. Let $\Omega_l(t_m)$

denote the region affected by the lth type of physical constraint during time interval t_m, with a severity coefficient $\alpha_l \in [0, 1]$. The overlap ratio between the constraint region and the effective portion of the grid cell is defined as

$$p_{il}(t_m) = \frac{| g_i^{\Omega} \cap \Omega_l(t_m) |}{| g_i^{\Omega} |} \tag{5}$$

and the combined physical-constraint effect and physical availability are

$$r_i(t_m) = 1 - \prod_{l=1}^{L} \left[1 - \alpha_l \frac{\left| g_i^{\Omega} \cap \Omega_l(t_m) \right|}{\left| g_i^{\Omega} \right|} \right] \tag{6}$$

$$\mu_i(t_m) = 1 - r_i(t_m) \tag{7}$$

where $\mu_i(t_m) \in [0, 1]$, with larger values indicating greater physical availability.

(2) Meteorological availability, denoted by $\kappa_i(t_m)$, describes the effect of weather conditions on the operational availability of an SRE.

Let $w_{ik}(t_m)$ denote the normalized risk indicator of the kth meteorological factor for a given resource element, and let the risk-mapping function $\phi_k(\cdot)$ convert this indicator into an impact intensity within [0, 1]. The combined meteorological effect and the resulting meteorological availability are defined as

$$\eta_i(t_m) = 1 - \prod_{k=1}^{K} (1 - \phi_k(w_{ik}(t_m)) \tag{8}$$

$$\kappa_i(t_m) = 1 - \eta_i(t_m) \tag{9}$$

where $\kappa_i(t_m) \in [0, 1]$, with larger values indicating more favourable meteorological conditions.

(3) Surveillance coverage, denoted by $\gamma_i(t_m)$, represents the effective surveillance support available to an SRE. Let $p_{is}^{\mathrm{cov}}(t_m) \in [0, 1]$ denote the effective single-source coverage provided by surveillance node $s\mathrm{SRE}_{i,m}$. Assuming approximately independent coverage among multiple surveillance nodes, the combined surveillance coverage is

$$\gamma_i(t_m) = 1 - \prod_{s=1}^{S} [1 - p_{is}^{\mathrm{cov}}(t_m)] \tag{10}$$

The formulation is independent of the specific single-sensor coverage model; a joint model may replace Equation (10) when substantial dependence among surveillance sources exists.

3.2.2. Resource-Feasibility Gating and Potential Supply

Physical availability, meteorological availability, and surveillance coverage jointly determine whether an SRE satisfies the minimum conditions required to form an effective resource supply. The resource-feasibility state is defined as

$$E_i(t_m) = \begin{cases} 1, \mu_i(t_m) \geq \mu_0,\ \kappa_i\ (t_m) \geq \kappa_0,\ \gamma_i\ (t_m) \geq \gamma_0 \\ 0, otherwise \end{cases} \tag{11}$$

where μ_0, κ_0, and γ_0 denote the minimum operating thresholds for the physical, meteorological, and surveillance attributes, respectively. The hard-threshold gate is used solely to determine whether an SRE satisfies the minimum operational-feasibility requirements; it is

not intended to represent continuous performance degradation. Direct aircraft occupancy and additional demand generated by task interactions belong to the demand side and therefore do not enter the resource-supply gate.

For an SRE that passes the feasibility gate, its effective potential resource supply is defined as

$$Q_i^{\sup}(t_m) = u_i^{\Omega} E_i(t_m)\left[w_\mu \mu_i(t_m) + w_\kappa \kappa_i(t_m) + w_\gamma \gamma_i(t_m)\right] \tag{12}$$

where w_μ, w_κ, and w_γ are weighting coefficients satisfying

$$w_\mu + w_\kappa + w_\gamma = 1 \tag{13}$$

$$Q_{i,gate}^{sup}(t_m) = u_i^{\Omega}\ E_i\ (t_m) \tag{14}$$

$$Q_{i,weight}^{sup}(t_m) = u_i^{\Omega}[w_\mu \mu_i(t_m) + w_\kappa \kappa_i(t_m) + w_\gamma \gamma_i(t_m)] \tag{15}$$

The potential resource supply satisfies $0 \le Q_i^{sup}(t_m) \le u_i^{\Omega} \le 1$. When $E_i(t_m) = 0$, the SRE cannot form an effective resource supply. When an SRE lies entirely within the study domain and all three supply attributes attain a value of 1, its potential supply reaches 1 SRE-eq.

Three ablation modes are considered to isolate the roles of minimum-feasibility gating and continuous supply-quality weighting: binary gating, continuous weighting, and the complete framework. All task-demand, local-matching, and aggregation procedures are held fixed across the three modes.

The thresholds and weighting coefficients may be determined from operational safety standards, historical operational data, structured expert weighting, or data-driven calibration. To ensure comparability among scenarios, all parameters are fixed before scenario comparison and their effects are subsequently evaluated through sensitivity analysis.

3.3. Task Resource Demand

After the potential resource supply of each SRE is obtained, the trajectories, operational protection envelopes, and local interaction states of a given task set need to be mapped onto task resource demand at the same resource-element scale. In this study, the direct spatio-temporal occupancy of tasks at the resource-element scale is taken as the baseline demand and is further extended through an optional interaction term to obtain the composite task resource demand.

Let the task set within the evaluation time window be $M = \{1, 2, \ldots, N_M\}$. For task $k \in M$, let $x_k(\tau)$ denote its trajectory position at time τ, and let $\mathcal{P}_k(\tau)$ denote its operational protection set. The effective occupancy region of the task is represented by the protection envelope as

$$\mathbf{B}_k(\tau) = \mathbf{x}_k(\tau) \oplus \mathcal{P}_k(\tau) \tag{16}$$

where $\oplus$ denotes the Minkowski sum. The protection set used for SRE demand mapping is a model-level occupancy envelope that represents local task influence and trajectory uncertainty at the resource-element scale. It should not be interpreted as an operational separation minimum. In particular, this SRE occupancy representation is distinct from the aircraft-level 3 NM/1000 ft separation criterion used in the independent trajectory-based benchmark introduced in Section 4.4.1.

The direct occupancy ratio of resource element $SRE_{i,m}$ by task k during time slice I_m is defined as

$$o_{ki}(t_m) = \frac{1}{|\mathbf{g}_i|\Delta t_m} \int_{t_m}^{t_{m+1}} \left|\mathbf{B}_k(\tau) \cap \mathbf{g}_i^{\Omega}\right| \mathrm{d}\tau \tag{17}$$

where $|\mathbf{B}_k(\tau) \cap \mathbf{g}_i \cap \Omega|$ denotes the overlap volume between the task protection envelope and spatial grid cell $\mathbf{g}_i$ within the study airspace at time τ. Here, $\Delta t_m = t_{m+1} - t_m$. The

quantity $o_{ki}(t_m)$ simultaneously captures the spatial coverage of the task protection envelope and the duration of its occupancy within the time slice, and satisfies $0 \leq o_{ki}(t_m) \leq u_i^{\Omega}$. The cumulative direct occupancy of task set M on the resource element is defined as

$$O_i(t_m|M) = \sum_{k \in M} o_{ki}(t_m) \tag{18}$$

Because multiple tasks may simultaneously compete for the same local spatio-temporal resource, $O_i(t_m|M)$ may exceed the maximum nominal supply u_i^{Ω} of a single resource element. Such an excess reflects competition among multiple tasks for limited local resources rather than repeated provision of the same spatial resource. By retaining cumulative demand at the resource-element scale, the model can distinguish spatial congestion caused by local resource competition from capacity loss caused by a system-wide reduction in resource supply.

3.4. Local Supply–Demand Matching Metrics

Potential resource supply and task resource demand are first matched locally at the SRE level before any spatial aggregation. This local-matching-first strategy preserves the original correspondence between resource availability and operational demand, allowing localized resource shortages and overload states to be identified even when sufficient resources exist elsewhere in the study region. In contrast, direct aggregation of supply and demand over the entire airspace may mask local shortages because surplus resources in unconstrained regions can compensate for insufficient resources in highly demanded regions.

3.4.1. Local Matching

The residual resource and local overload of each resource element are defined as

$$Q_i^{\text{res}}(t_m \Big| M) = \left[Q_i^{\text{sup}}(t_m) - D_i(t_m \mid M) \right]^+ \tag{19}$$

$$H_i(t_m \Big| M) = \left[D_i(t_m \mid M) - Q_i^{sup}(t_m) \right]^+ \tag{20}$$

where + denotes the positive-part operator. $H_i(t_m|M) > 0$ indicates that local task demand exceeds potential resource supply. In particular, when $Q_i^{\text{sup}}(t_m) = 0$ and $D_i\ (t_m|M) > 0$, $H_i(t_m|M) = D_i\ (t_m|M)$.

The local resource-accounting relationship is therefore maintained as

$$Q_i^{\text{sup}}(t_m) + H_i(t_m \mid M) = D_i(t_m \mid M) + Q_i^{res}(t_m) \tag{21}$$

This relationship ensures that resource surplus and unmet demand are explicitly separated at the local spatio-temporal scale, and the aggregation of local states does not eliminate spatially constrained shortages.

Within each time slice, the corresponding aggregate quantities are

$$\begin{aligned} C^{\text{sup}}(t_m) &= \sum_{i=1}^{N} Q_i^{\text{sup}}(t_m) \\ C^{D}(t_m|M) &= \sum_{i=1}^{N} D_i\ (t_m|M) \\ C^{\text{res}}(t_m|M) &= \sum_{i=1}^{N} Q_i^{res}\ (t_m|M) \end{aligned} \tag{22}$$

$C^{\text{sup}}(t_m)$ is defined as the SRE-based available resource capacity at time t_m. It represents the total effective spatio-temporal resource supply available within the evaluated airspace under the current operational environment and is expressed in SRE-eq. In contrast,

$C^D(t_m \mid M)$ represents the aggregated resource demand imposed by the task set, while $C^{\text{res}}(t_m|M)$ represents the residual resource capacity after local supply–demand matching.

For an individual time slice t_m, the spatially aggregated local overload is:

$$H_{local}(t_m|M) = \sum_{i=1}^{N} H_i(t_m|M) \tag{23}$$

$$H_{local}^{cum}(M) = \sum_{m} \sum_{i=1} H_i(t_m|M) \tag{24}$$

$H_{local}(t_m|M)$ is the spatially aggregated local-overload magnitude for an individual time slice, whereas $H_{local}^{cum}(M)$ is its cumulative value over the evaluation period. Both are expressed in SRE-eq. These quantities diagnose the magnitude of local resource–demand imbalance and should not be interpreted as aircraft-count capacity values or calibrated operational capacity thresholds.

3.4.2. Local Versus Global Aggregation

To evaluate the influence of spatial correspondence between resource supply and task demand, a global aggregation-based shortage is additionally defined:

$$H_{global}(t_m) = [\sum_{m} \sum_{i} D_i(t_m|M) - \sum_{m} \sum_{i} Q_i^{sup}(t_m)]^+ \tag{25}$$

Unlike local matching, H_{global} performs supply–demand comparison only after spatial aggregation, and shortages occurring in resource-limited regions may be compensated by unused resources from other regions.

The difference between local and global shortages is defined as

$$\Delta H = H_{local} - H_{global} \tag{26}$$

where ΔH represents the amount of locally constrained demand that is concealed by global aggregation.

Because local matching preserves SRE-level supply–demand correspondence before aggregation, $H_{local} \geq H_{global}$, under identical supply and demand conditions.

This difference provides a direct measure of the limitation of conventional aggregated capacity assessment and enables the identification of operational states with identical global resource conditions but different local feasibility. Reported time-averaged metrics are arithmetic means over all analysis time slices.

The reference maximum cumulative resource amount of the study domain is

$$C_{\text{ref}} = \sum_{i=1}^{N} u_i^{\Omega} \tag{27}$$

To support relative comparisons among different regions and scenarios under the same SRE specification, and to facilitate assessment of result stability under different grid configurations, the following normalized metrics are defined

$$I^{\text{sup}}(t_m) = \frac{C^{\text{sup}}(t_m)}{C_{\text{ref}}} \tag{28}$$

$$I^{\text{res}}(t_m|M) = \frac{C^{\text{res}}(t_m|M)}{C_{\text{ref}}} \tag{29}$$

Both metrics are dimensionless. $I^{\text{sup}}(t_m)$ is the normalized SRE-based resource-capacity index, representing the fraction of reference resource capacity that remains available un-

der the current operational environment. $I^{\mathrm{res}}(t_m|M)$ represents the normalized residual resource-capacity state after accounting for task demand. These normalized indices facilitate comparisons across operating scenarios under a common SRE specification. When different discretization scales are compared, normalized indices or relative rates of change are used rather than raw SRE-eq total. To quantify the spatial extent of overload within the area of active task demand, the overload proportion of the active-demand region is defined as

$$P_{\mathrm{over}}^{\mathrm{act}}(t_m|M) = \frac{\sum_{i=1}^{N} u_i^{\Omega} 1\left[D_i(t_m\middle|M) > Q_i^{\mathrm{sup}}(t_m)\right]}{\sum_{i=1}^{N} u_i^{\Omega} 1[D_i(t_m|M) > 0]} \tag{30}$$

When no task demand exists within a time slice, and the denominator is zero, $P_{\mathrm{over}}^{\mathrm{act}}(t_m|M) = 0$.

$P_{\mathrm{over}}^{\mathrm{act}}$ represents the geometrically weighted proportion of the active-demand region in which local task demand exceeds available resource supply. The indicator is dimensionless and bounded in [0, 1]. It is a deterministic descriptor of the spatial extent of local resource–demand overload and should not be interpreted as a stochastic aircraft-conflict probability or as a calibrated operational capacity threshold. When no active task demand exists in a time slice, the denominator is zero and $P_{\mathrm{over}}^{\mathrm{act}}$ is set to zero.

To characterize the spatial organization of active task demand, a dimensionless concentration index C is defined as the Gini coefficient of the demand values over active SREs:

$$C = \frac{2\sum_{k=1}^{n} kD_{(k)}}{n\sum_{k=1}^{n} D_{(k)}} - \frac{n+1}{n} \tag{31}$$

where the demand values of the active SREs are sorted in ascending order. C corresponds to a perfectly uniform distribution of active demand, whereas larger values indicate stronger spatial concentration.

4. Case Study and Validation

4.1. Study Area and Data Description

The terminal airspace surrounding Amsterdam Airport Schiphol (EHAM) was selected as the case-study area. Schiphol is one of the busiest airports in Europe and operates under complex terminal-area conditions involving dense arrival and departure flows, multiple runway configurations, and frequent interactions between different traffic streams. These characteristics make it an appropriate case-study area for investigating spatially heterogeneous resource availability and localized capacity constraints in terminal airspace operations.

The horizontal boundary of the study area extends from 3.95° E to 5.45° E and from 51.55° N to 53.05° N, with a vertical range from ground level to 12,000 m. Following the SRE definition introduced in Section 3.1, the terminal airspace is discretized into three-dimensional spatial elements. A horizontal grid of 30 × 30 cells and five vertical layers are adopted, with a temporal resolution of 5 min. Under this configuration, the 3 h analysis period contains 36 time intervals and 162,000 spatio-temporal resource elements.

Historical aircraft trajectories are obtained from the OpenSky Network. The selected traffic period is from 12:00 to 15:00 UTC on 12 June 2024. Aircraft states, including position, altitude, and temporal evolution, are extracted from ADS-B trajectories and mapped onto the corresponding SREs. A total of 30 active aircraft operating within the study region are identified during the analysis period.

Meteorological information is obtained from Open-Meteo records, including precipitation, cloud coverage, wind speed, wind direction, and weather codes. These variables

are used to construct spatially and temporally varying meteorological availability fields. Instead of directly modifying traffic demand, meteorological effects are incorporated into the resource-supply side, where adverse conditions reduce the effective availability of corresponding SREs. Surveillance coverage is retained as a general resource-supply component in the SRE formulation. In the present case study, however, surveillance conditions are held spatially and temporally constant across all comparison scenarios. Therefore, no independent surveillance-degradation scenario is considered here, and the specific effect of surveillance variation is outside the scope of the present evaluation. For the SRE-independent trajectory-based feasibility assessment, an additional aircraft-level 4D trajectory library was constructed from historical adsb.lol trajectory archives over the same 12:00–15:00 UTC analysis window. Fifty daily archives satisfying the complete-trajectory quality-control requirements were retained, yielding 13,798 observed aircraft trajectories. Each aircraft was preserved as an individual object containing timestamp, latitude, longitude, and altitude information. The trajectories were resampled onto a common 5 s temporal grid, while interpolation was not performed across data gaps exceeding 60 s. The original observed temporal positions of the trajectories within the analysis window were retained; no artificial time shifting was introduced in the independent benchmark.

Three complementary evidence layers are used in the present study. First, observed ADS-B trajectories and meteorological records provide the empirical operational background for the baseline Schiphol case. Second, controlled parameterized experiments modify resource availability, demand–resource spatial correspondence, and traffic organization while holding other relevant conditions fixed; these experiments are designed to isolate individual mechanisms rather than reproduce independently observed capacity-restriction events. Third, an aircraft-level 4D trajectory benchmark is evaluated independently of the SRE resource-accounting formulation to examine whether SRE-derived local overload is consistent with separation-constrained operational feasibility. Additional observed traffic periods are further used to assess cross-period robustness. Accordingly, the evidence is interpreted as a combination of mechanism-oriented controlled evaluation, SRE-independent trajectory-based feasibility validation, and cross-period robustness assessment, rather than as direct validation against an independently observed terminal airspace capacity value.

4.2. Validation Framework

To examine the diagnostic behaviour of the proposed framework under controlled conditions, this study designs three groups of scenario-based evaluation experiments addressing the following research questions:

(1) Whether resource-induced capacity degradation can be identified before traffic saturation occurs;
(2) Why identical global supply–demand states may lead to different local operational feasibility and whether spatially explicit resource accounting can reveal such hidden differences;
(3) How traffic spatial organization affects local capacity pressure under fixed resource and demand volumes.

Three groups of controlled experiments are constructed to isolate the above mechanisms. The first experiment explores resource-side capacity degradation under varying meteorological disturbances with a fixed traffic demand. The second experiment verifies the spatial non-substitutability of airspace resources by maintaining identical global supply–demand levels while altering their spatial correspondence. The third experiment investigates how different traffic spatial structures influence local operational pressure under unchanged resource conditions. By independently controlling resource availability,

spatial matching status, and traffic organization, the experiments reveal localized capacity constraints that cannot be captured by conventional aggregated metrics.

4.2.1. Weather-Induced Resource Degradation

Weather disturbance is a primary driver of dynamic terminal capacity variation and imposes spatially heterogeneous resource constraints. Localized precipitation, reduced visibility, strong winds, or temporary operational restrictions can degrade airspace availability in specific regions while leaving other areas unaffected.

To identify resource-induced capacity loss before traffic saturation, multiple controlled weather scenarios are established. A clear-sky condition is adopted as the baseline, and different disturbance intensities are generated by adjusting the meteorological resource availability field, with disturbance values ranging from 0.55 to 0.80. All traffic trajectories, aircraft volumes, and operational settings remain unchanged during the simulation. Instead of replicating specific real-world weather events, this experiment aims to detect latent capacity degradation caused solely by resource reduction. The variations in normalized resource supply and residual resource availability are analyzed to examine how the SRE framework responds to weather-induced resource degradation under controlled conditions.

4.2.2. Spatial Non-Substitutability of Airspace Resources

Traditional aggregated capacity methods implicitly assume spatial substitutability, namely that resource surplus in one region can offset resource shortages elsewhere. However, terminal airspace operations are spatially constrained, and aircraft operations require locally available spatio-temporal resources, making cross-region resource substitution infeasible in most cases.

This experiment compares paired scenarios with identical global traffic demand, total resource supply, and global supply–demand ratios. The only controlled variable is the spatial matching degree between traffic distribution and resource availability. In the spatially matched scenario, high-demand areas overlap with sufficient airspace resources. In the mismatched scenario, traffic is redistributed toward resource-limited regions while maintaining identical overall demand and supply volumes.

Since global operational conditions remain unchanged, any discrepancy in operational feasibility purely originates from spatial supply–demand mismatch. Within this controlled setting, the experiment examines whether local resource–demand accounting can reveal spatially constrained shortages that are obscured by global aggregation.

4.2.3. Influence of Traffic Spatial Organization on Local Operational Feasibility

Even with identical traffic volumes and resource availability, different traffic spatial distributions lead to distinct resource competition patterns and varying operational pressures. Traffic spatial organization therefore constitutes a critical but underexplored factor affecting dynamic terminal capacity.

Three typical traffic organizational patterns, namely clustered, uniform, and crossing configurations, are constructed for controlled comparison. All scenarios share the same total aircraft volume, meteorological conditions, and SRE-based resource supply, while only the spatial layout of flight trajectories differs. The clustered pattern represents concentrated traffic distribution, the uniform pattern denotes evenly spread demand, and the crossing pattern reflects intersecting traffic flows with intensive local interactions. Comparative analysis focuses on local-overload distribution, interaction intensity, and spatial operational pressure. This controlled experiment examines how traffic spatial organization alters local operational pressure even when total demand and resource conditions remain unchanged.

4.3. Comparison with Conventional Airspace Representations

To investigate the limitations of existing capacity representations, three commonly used indicators are selected as references: aircraft count, traffic density, and spatio-temporal occupancy.

Aircraft count represents the overall traffic volume within the terminal area and is widely used as a basic loading indicator. However, it does not consider differences in trajectory characteristics, residence time, or resource consumption among aircraft operations. Traffic density extends aircraft count by incorporating spatial concentration information. Although it provides additional information regarding traffic distribution, it primarily describes the demand side of airspace operations and does not explicitly consider the availability of operational resources. The occupancy-based representation considers the temporal and spatial occupation of airspace cells using the same discretization framework as the proposed method. This comparison is introduced to distinguish the contribution of SRE-based resource accounting from simple trajectory-occupancy representation.

For a fair comparison, all conventional indicators are calculated using identical trajectory data, spatial domains, and temporal resolutions. The comparison results are analysed under the three experimental scenarios described in Section 4.2. These indicators represent typical demand-oriented and occupancy-based approaches in current airspace capacity assessment. Their comparison with the proposed SRE framework provides insight into whether explicit resource–demand interaction modelling introduces additional information beyond existing capacity representations.

4.4. Evaluation Metrics and Analysis Procedure

The evaluation combines the SRE diagnostic metrics defined in Section 3.4 with an independent aircraft-level trajectory benchmark. For the weather-degradation experiment, normalized resource-supply and residual-resource indices are used to characterize resource-side deterioration under fixed traffic demand. For the spatial non-substitutability experiment, globally aggregated shortage measures are compared with time-averaged local SRE overload under identical total supply and demand. For the traffic-organization experiment, local overload, active-region overload proportion, and demand concentration are used to characterize the magnitude, spatial extent, and concentration of local demand pressure. In addition, Section 4.4.1 introduces an SRE-independent trajectory-based operational-feasibility benchmark, while Section 4.4.2 evaluates the sensitivity of the SRE results to discretization and model parameters.

4.4.1. Independent Trajectory-Based Operational-Feasibility Benchmark

To provide an operational-feasibility reference that is methodologically independent of the SRE resource-accounting formulation, an aircraft-level 4D trajectory benchmark was constructed. The benchmark operates directly on complete trajectories and does not use SRE resource supply, SRE-eq demand, residual-resource indices, local-overload quantities, or any SRE-derived feasibility threshold.

The trajectory library contains 13,798 complete aircraft trajectories obtained from 50 daily ADS-B archives satisfying the trajectory quality-control requirements. Each trajectory retains timestamp, latitude, longitude, and altitude information, and is resampled onto a common 5 s temporal grid. Interpolation is not performed across temporal gaps exceeding 60 s. The observed timing of each trajectory within the 12:00–15:00 UTC analysis window is retained. Candidate demand levels are defined as

$$N \in \{50, 100, 150, 200, 250, 300, 350\} \tag{32}$$

Fifty Monte Carlo realizations are generated. For each realization, a candidate set of 350 complete trajectories is sampled first, and the lower-demand levels are formed as nested prefixes of the same trajectory set. This nested design ensures that changes across demand levels arise from increasing candidate demand rather than from unrelated trajectory samples.

For any pair of aircraft i and j with temporally overlapping trajectories, let $d^i_H j(t)$ and $d^i_V j(t)$ denote their horizontal and vertical separation distances at time t, respectively. A pairwise separation conflict is defined as

$$c_{ij} = \left[\exists t \in T_i \cap T_j : d^{ij}_H(t) < D_H \ \wedge \ d^{ij}_V(t) < D_V\right] \tag{33}$$

where the primary criterion is D_H = 3 NM and D_V = 1000 ft. A more conservative 5 NM/1000 ft criterion is additionally evaluated as a sensitivity case.

For each demand level N, a conflict graph $G_N = (V_N, E_N)$ is constructed, where each candidate aircraft corresponds to one vertex and an edge $(i,j) \in E_N$ is introduced whenever $c_{ij} = 1$. The maximum conflict-free subset is obtained using the following binary optimization:

$$T_{ind}(N) = \max_x \sum_{i=1}^{N} x_i, \text{ s.t. } x_i + x_j \leq 1, \ \forall (i,j) \in E_N, \ x_i \in \{0,1\} \tag{34}$$

where $x_i = 1$ indicates that candidate trajectory i is retained in the conflict-free subset. $T_{ind}(N)$ therefore represents the separation-constrained feasible throughput of the candidate trajectory set under fixed observed trajectories. It should not be interpreted as an independently observed ATC capacity value because controller intervention, rerouting, delay assignment, and trajectory modification are not represented.

Two additional quantities are defined as

$$A(N) = \frac{T_{ind}(N)}{N}, \ U_{ind}(N) = N - T_{ind}(N) \tag{35}$$

where $A(N)$ is the feasible acceptance ratio and U_{ind} is the independently rejected demand.

The same trajectory realizations are subsequently mapped into the SRE framework, independently of the trajectory-based conflict calculation, to obtain H^{cum}_{local}, P^{act}_{over} and I_{res}. Agreement between the two computational chains is assessed only after both chains have been completed. Because both U_{ind} and SRE overload increase with candidate demand, the association analysis includes a demand-adjusted Spearman assessment controlling for N, a partial-rank analysis controlling for N, and within N Spearman coefficients. Robustness of the independent benchmark is additionally examined using 5, 10, and 20 s resampling intervals and the alternative 5 NM/1000 ft separation criterion.

4.4.2. Sensitivity-Analysis Procedure

Because the SRE-based diagnostic quantities depend on the adopted spatio-temporal discretization and model parameters, a sensitivity analysis was conducted to examine whether the principal mechanism-level conclusions are robust to these modelling choices. The baseline configuration summarized in Table 1 was used as the reference. Four groups of alternative settings were examined: (1) horizontal grid resolutions of 20 × 20 and 40 × 40 cells relative to the 30 × 30 baseline; (2) temporal resolutions of 2.5 and 10 min relative to the 5 min baseline; (3) three alternative supply-weight combinations, w = [0.6, 0.2, 0.2], w = [0.6, 0.2, 0.2], and w = [0.2, 0.2, 0.6]; and (4) simultaneous ±20% perturbations of the resource-feasibility thresholds relative to their baseline values. All other SRE-model settings were held fixed during each sensitivity test.

Table 1. Baseline SRE model parameters and settings used in the controlled case-study experiments.

Parameter	Symbol	Baseline Value
Horizontal grid	–	30 × 30 cells
Vertical layers	–	5
Time step	Δt	5 min
Resource-feasibility gating	$(\mu_0 \backslash \kappa_0 \backslash \gamma_0)$	(0.60\0.55\0.55)
Physical/meteorological/surveillance weights	$(w_\mu \backslash w_\kappa \backslash w_\gamma)$	(1/3\1/3\1/3)
Density/complexity weights	(α_D, α_C)	(0.40, 0.60)
Interaction coefficient	β_σ	0.30
Squall-line band width	B_W	6.0 cells
Maximum supply reduction	–	0.95
Altitude-decay coefficient	–	0.35
Regional availability	R1/R2/R3	0.00/0.15/0.40
Sensor network	–	8 sensors, fixed in time
Coverage floor	–	0.15

Robustness was evaluated using the normalized clear-weather resource-capacity index I_{sup}^{Clear}, the matched–mismatched overload difference ΔH under moderate weather, the ordering of the weather-degradation scenarios, and the sign of ΔH. Because raw SRE-eq totals depend on discretization, emphasis is placed on normalized or relative quantities and on preservation of qualitative scenario relationships rather than invariance of absolute values.

5. Results

5.1. Weather-Induced Resource Degradation Under Unchanged Traffic Demand

Dynamic terminal airspace capacity is often assessed using traffic-demand-related indicators, such as aircraft count, traffic density, or occupancy level. These indicators implicitly assume that capacity degradation becomes apparent only when traffic demand approaches the operational limit. However, in practical operations, available airspace resources may deteriorate under adverse conditions before traffic demand increases, resulting in a latent reduction in operational capacity that cannot be directly reflected by conventional demand-oriented metrics.

To investigate this issue, a weather-induced resource degradation experiment was conducted. Four weather conditions, including normal, mild, moderate, and severe degradation scenarios, were considered. During the experiment, the traffic demand was strictly controlled to remain unchanged, with the same aircraft number and spatial-temporal distribution applied across all scenarios. Therefore, any variation in capacity-related performance was attributed to changes in available airspace resources rather than changes in traffic demand.

As shown in Figure 2a, the parameterized weather degradation progressively reduces the normalized resource-supply level from 100% under the normal condition to 70% under the severe condition. The traffic input is deliberately held fixed across all four scenarios: the same aircraft count and the same spatio-temporal trajectory distribution are used in each case, as illustrated in Figure 2b. Accordingly, the conventional demand-oriented indicators shown in Figure 2c remain unchanged and overlap because they are calculated from the same fixed traffic input. In contrast, the model-derived SRE resource-availability indicator decreases as the parameterized weather condition becomes more restrictive (Figure 2d). This controlled comparison therefore isolates the response of the framework to resource-side degradation while excluding changes in traffic demand.

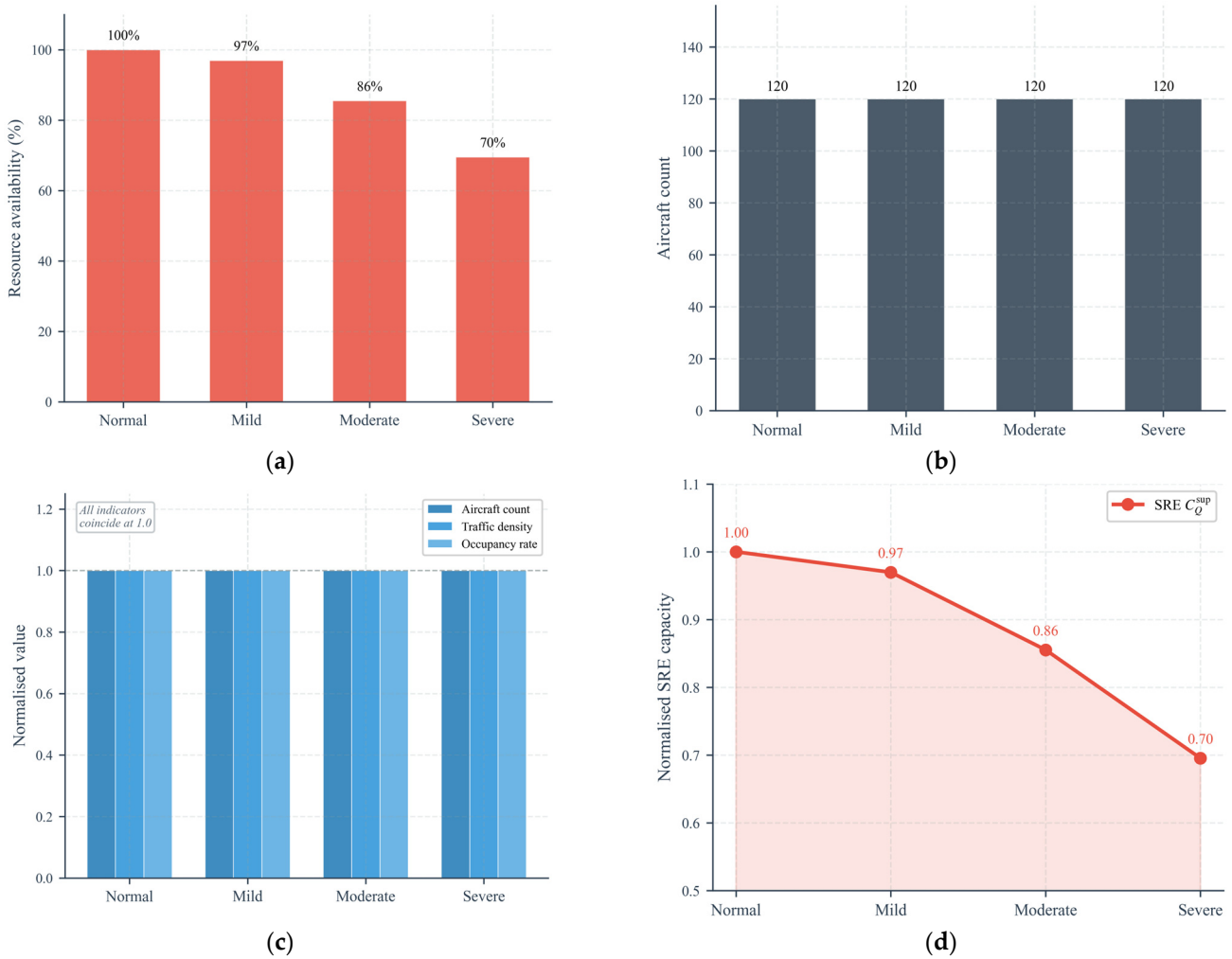


Figure 2. Weather-induced resource degradation under unchanged traffic demand: (**a**) variation in available airspace resources under different weather conditions; (**b**) constant traffic demand maintained across scenarios; (**c**) response of conventional demand-oriented indicators; and (**d**) SRE-based capacity variation under resource degradation. The shaded area in subplot (**d**) represents the range of normalized SRE capacity.

To provide an aircraft-count-based interpretation of the SRE-based resource-capacity variation, the throughput-equivalent procedure described in Section 4.4.1 was applied. Aircraft demand was increased from 50 to 350 aircraft in increments of 50 while the underlying trajectory-expansion procedure was kept unchanged. As shown in Figure 2a, the time-averaged demand-to-supply ratio increases progressively with aircraft demand, while stronger weather degradation causes the predefined feasibility threshold of 0.80 to be reached at a lower demand level. According to this criterion, the throughput-equivalent capacity is 250 aircraft under clear-sky and mild conditions, decreases to 200 aircraft under moderate degradation, and further decreases to 150 aircraft under severe degradation (Figure 2b). Figure 2c further shows a strong association between the SRE-based resource-capacity measure and the corresponding throughput-equivalent capacity across the four weather conditions. Because both quantities are derived within the same SRE-based resource-accounting framework, this relationship is interpreted as an internal consistency result rather than as independent external validation. In contrast, the conventional traffic-density indicator increases almost linearly with aircraft demand and remains identical across weather conditions (Figure 2d), because it does not explicitly account for weather-induced changes in resource availability.

As shown in Figure 3a, increasing weather-degradation severity progressively reduces the prescribed resource-availability level, while the traffic input is held fixed across all four scenarios. The same aircraft set and spatio-temporal demand distribution are therefore used under clear, mild, moderate, and severe conditions. Consequently, the conventional demand-oriented indicators in Figure 3c remain unchanged because they depend only on the fixed traffic input. In contrast, the model-derived normalized SRE resource-capacity state decreases as the prescribed meteorological constraints become more restrictive (Figure 3d). Under the severe-weather setting, I_{sup} decreases by 27.8% relative to the clear-weather baseline. This controlled comparison shows that the SRE framework can identify resource-side deterioration even when traffic demand itself does not change.

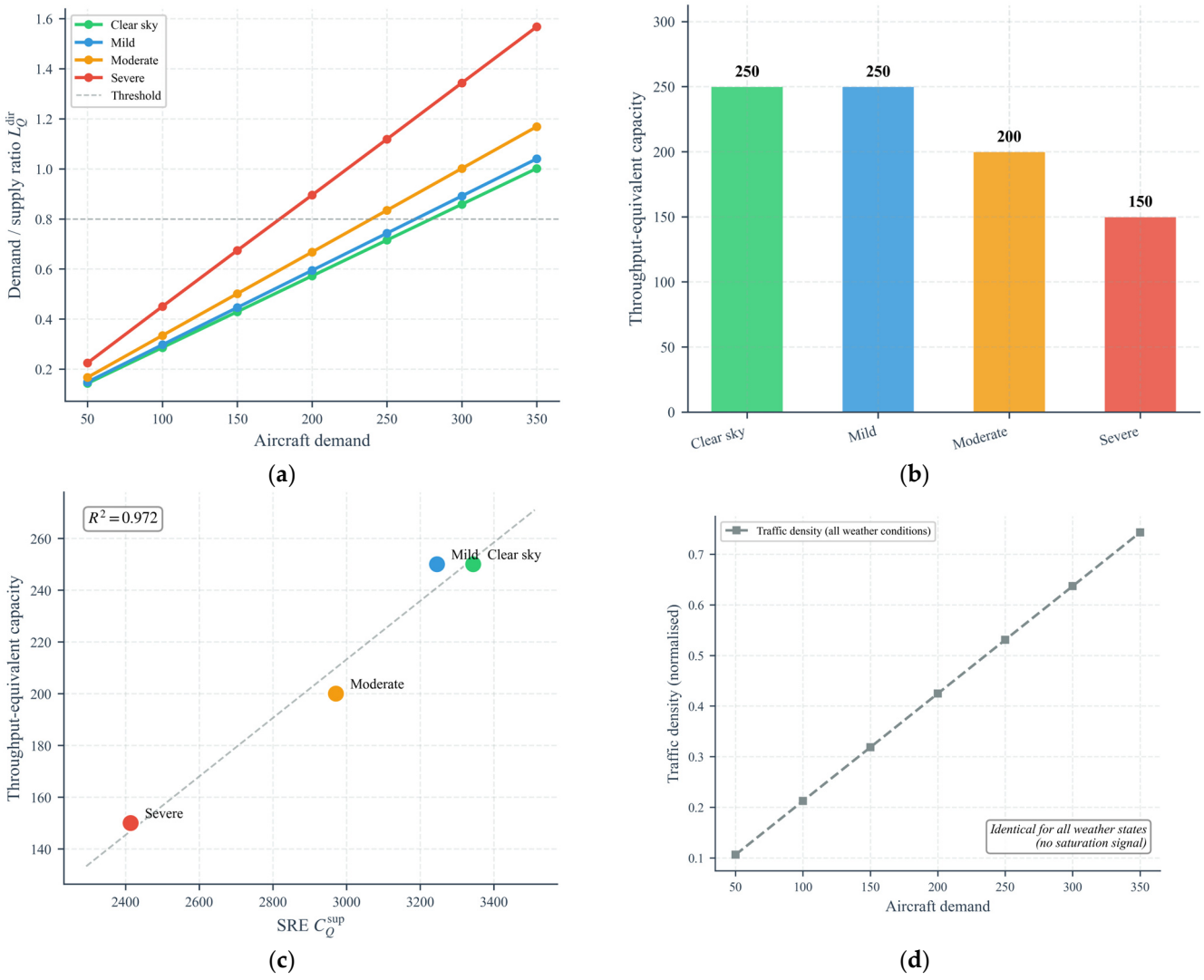


Figure 3. Controlled evaluation of resource-side degradation under fixed traffic demand: (**a**) parameterized resource-supply levels under different weather-degradation conditions; (**b**) fixed aircraft count based on the common traffic input used across all scenarios; (**c**) conventional demand-oriented indicators calculated from the unchanged traffic input, with overlapping curves reflecting their identical responses; and (**d**) model-derived SRE resource-availability response to parameterized resource degradation.

5.2. Independent Trajectory-Based Operational-Feasibility Validation

To evaluate whether SRE-derived local overload is consistent with an operational-feasibility measure that is independent of the SRE accounting formulation, fifty Monte

Carlo realizations were evaluated at each demand level using nested candidate sets and complete aircraft-level 4D trajectories.

Under the primary 3 NM/1000 ft criterion, median independent feasible throughput T_{ind} increased from 44 aircraft at N = 50 to 207 aircraft at 305 (Figure 4a). The corresponding interquartile ranges remained comparatively narrow, ranging from 42–45 aircraft at N = 50 to 204–212 aircraft at 350. However, the increase in T_{ind} was sublinear relative to candidate demand. Accordingly, the feasible acceptance ratio $A(N)$ decreased monotonically from 0.88 to 0.59 as N increased (Figure 4b). Under the more conservative 5 NM/1000 ft criterion, feasible-throughput estimates were consistently lower, decreasing from 41 accepted aircraft at N = 50 relative to the primary criterion and reaching 175 aircraft at N = 350. No saturation plateau was observed within the tested range up to 350 candidate aircraft; therefore, this experiment does not infer a single operational-capacity threshold.

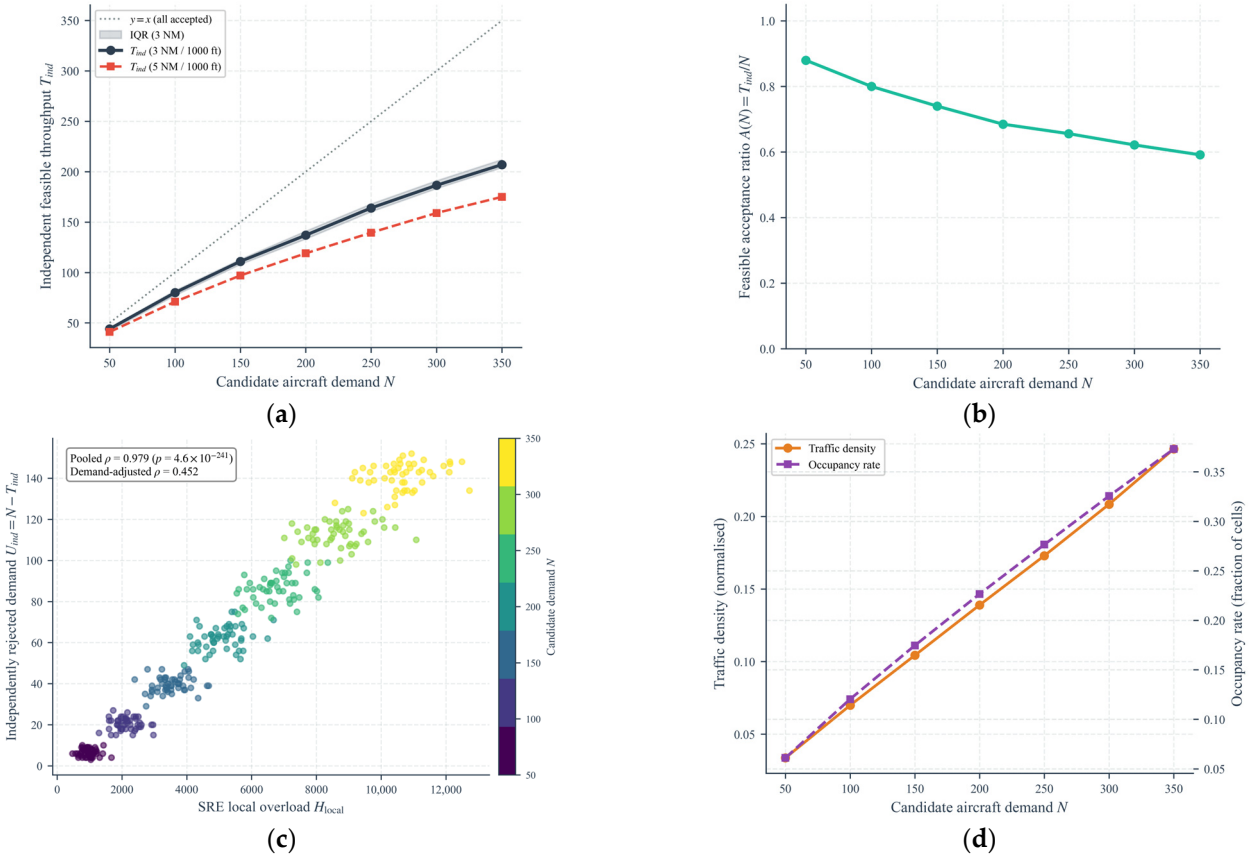


Figure 4. Independent trajectory-based operational-feasibility assessment and its relationship with SRE-derived cumulative local overload. (**a**) Median independent feasible throughput T_{ind} as a function of candidate aircraft demand under the primary 3 NM/1000 ft and increased-sensitivity 5 NM/1000 ft separation criteria; the shaded band denotes the interquartile range for the primary criterion and the dotted $y = x$ line represents complete acceptance. (**b**) Feasible acceptance ratio under the primary criterion. (**c**) Relationship between independently rejected demand and cumulative SRE local overload H^{cum}_{local} across the Monte Carlo realizations. (**d**) Conventional traffic-density and occupancy-rate responses to increasing candidate demand.

The independently rejected demand U_{ind} was then compared with the cumulative SRE local overload H^{local}_{cum} calculated from the same trajectory realizations but through a separate computational chain. The pooled association was strong; however, because both quantities increase with candidate demand, the demand-adjusted analysis was treated as the primary association measure. After controlling for candidate demand, the association remained positive $\rho = 0.452$, $p = 4.9 \times 10^{-19}$. A partial-rank analysis controlling for demand provided

a smaller but still positive association $\rho = 0.171$, $p = 0.0013$. Within fixed demand levels, the association was negative when operational pressure was low, but became consistently positive at higher demand levels, with coefficients of approximately 0.19–0.28 for $N > 150$. These results indicate that realizations producing larger SRE-derived cumulative local overload also tend to require more trajectory removals under the independent separation-constrained benchmark, beyond the common effect of increasing aircraft demand.

The independent association was also robust to trajectory-resampling resolution. The demand-adjusted Spearman coefficient was 0.452, 0.457, and 0.436 under 5, 10, and 20 s resampling, respectively, while the within-N coefficient at $N = 350$ remained approximately 0.28–0.30. Figure 4d shows that conventional traffic-density and occupancy-rate indicators increase almost monotonically with candidate demand but do not themselves provide a separation-constrained feasibility estimate. Taken together, these results provide an SRE-independent operational-feasibility reference for interpreting local SRE overload, while not equating either quantity with independently observed ATC capacity.

5.3. Spatial Non-Substitutability of Airspace Resources Under Global Capacity Equivalence

Global capacity assessment approaches often use aggregated demand and resource totals. They assume that a surplus in one area can offset a deficit in another. Terminal airspace operations have spatial limits. Aircraft must be supported by local operational resources. So, substitution across regions may not always work. Therefore, identical global supply–demand figures do not necessarily mean the same operational feasibility.

To investigate this issue, paired scenarios were constructed with identical total traffic demand, total resource supply, and global demand-to-supply conditions. The only difference between the two scenarios was the spatial correspondence between traffic demand and available resources. As summarized in Table 1, both scenarios exhibit identical global capacity-related quantities, ensuring that the effect of spatial distribution can be isolated, as summarized in Table 2.

Table 2. Experimental settings for global capacity equivalence scenarios.

Condition	Spatially Matched	Spatially Mismatched
Total traffic demand (SRE-eq)	27.63	27.63
Total resource supply (SRE-eq)	10.02	10.02
Global demand-to-supply ratio	2.76	2.76
Global overload (H_{global})	22.90	22.90
Demand–resource spatial correspondence	Matched	Shifted toward low-resource regions

In the spatially matched condition, high-demand regions were aligned with areas providing sufficient resources. In contrast, in the spatially mismatched condition, demand was redistributed toward regions with relatively limited resource availability while maintaining the same global demand and supply levels.

As illustrated in Figure 5a,b, the two scenarios exhibit substantially different local demand–resource distributions despite identical global conditions. In the matched scenario, demand is generally supported by the corresponding local resource availability. However, the mismatched scenario produces concentrated regions with elevated demand–resource ratios, indicating localized resource competition that cannot be identified through global aggregation.

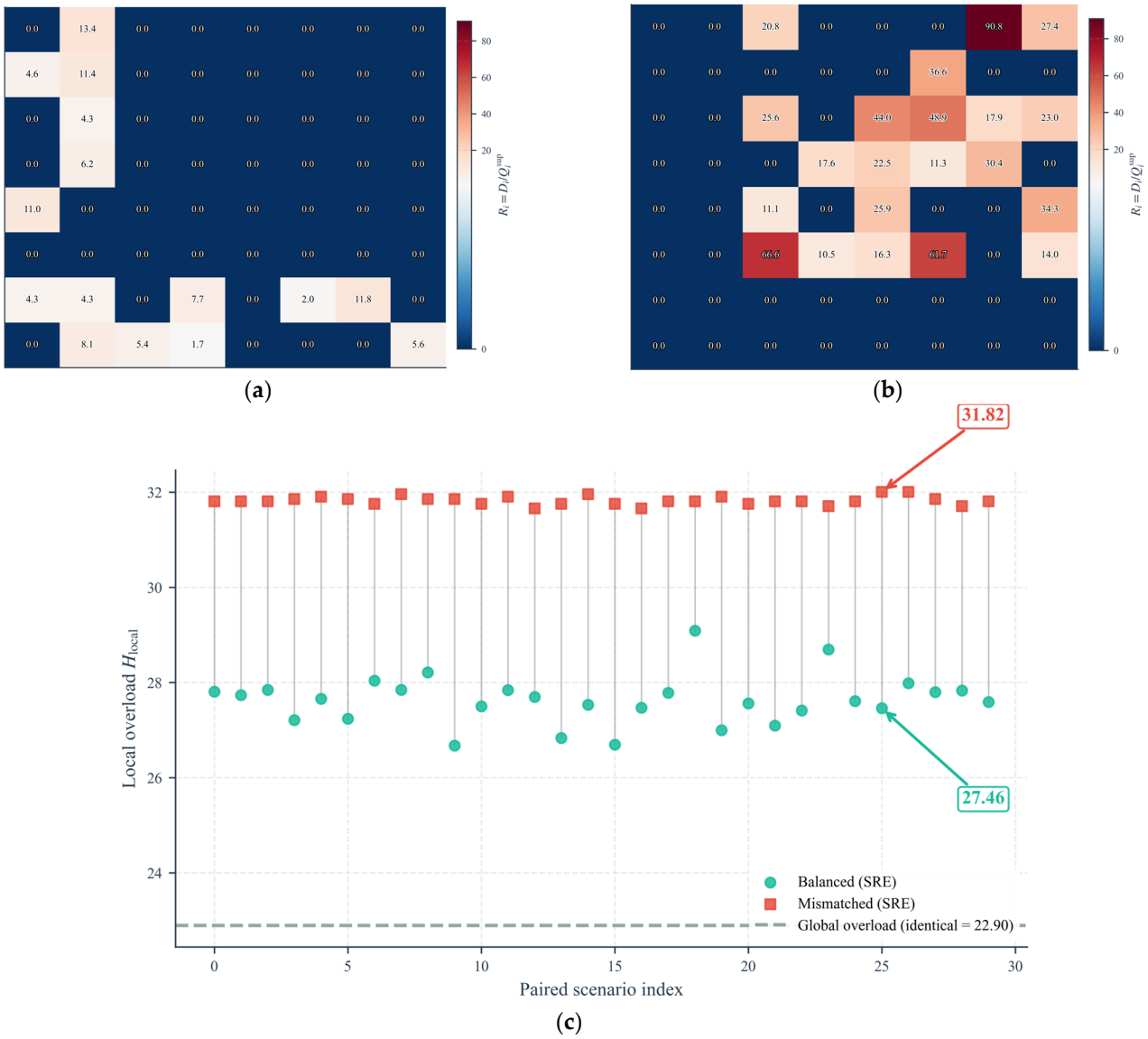


Figure 5. Spatial non-substitutability of airspace resources under identical global capacity conditions: (**a**) spatially matched demand–resource distribution; (**b**) spatially mismatched demand–resource distribution; and (**c**) paired comparison of local overload under identical global conditions.

The global indicators remain unchanged between the two scenarios, including the global demand-to-supply ratio and aggregated overload level. Furthermore, the paired comparison in Figure 5c demonstrates that the global overload remains identical across all generated scenario pairs, whereas the local SRE-based overload consistently increases under spatial mismatch. For the representative case, the local overload increases from 27.46 in the spatially matched condition to 31.82 in the spatially mismatched condition, corresponding to an increase of approximately 15.9%.

These results demonstrate that terminal airspace capacity is not solely determined by the total amount of available resources. Instead, operational feasibility depends strongly on the spatial correspondence between traffic demand and resource availability. Aggregating resources before considering their spatial accessibility may mask localized capacity constraints by allowing resource surpluses in unconstrained regions to offset shortages elsewhere. By preserving local supply–demand relationships, the proposed SRE framework provides a spatially explicit representation of capacity limitations that cannot be captured by global capacity indicators.

5.4. Influence of Traffic Spatial Organization on Local Operational Feasibility Under Identical Resource Conditions

Beyond resource-side degradation and spatial supply–demand mismatch, the spatial organization of aircraft movements can alter local operational pressure even when total traffic demand and available resources remain unchanged. This experiment therefore examines whether alternative traffic organization redistributes local resource competition under otherwise identical global conditions. Three representative traffic-organization patterns were constructed, including clustered, uniform, and crossing configurations. The total aircraft demand, weather conditions, and available SRE-based resource capacity were maintained identically across all scenarios, while only the spatial arrangement of traffic flows was modified. The corresponding experimental settings and quantitative results are summarized in Table 3.

Table 3. Experimental configurations and resulting SRE-based operational indicators under different traffic organization.

Traffic Organization	Aircraft Demand	Weather Condition	SRE Supply Capacity	Local Overload (H_{local})	Active-Region Overload Proportion (P_{over}^{act})	Concentration Index
Clustered	120	Moderate	2971.4	116.0	0.97	0.448
Uniform	120	Moderate	2971.4	110.9	0.97	0.314
Crossing	120	Moderate	2971.4	114.7	0.81	0.531

Only the spatial organization of traffic trajectories is varied among the three scenarios, while total aircraft demand, meteorological conditions, and resource-supply settings are held constant. Figure 6a shows the three constructed traffic-organization inputs. In the clustered scenario, trajectories are concentrated within a limited portion of the study area; in the uniform scenario, traffic demand is distributed more evenly; and in the crossing scenario, intersecting trajectory flows create localized interaction regions. Because total aircraft demand and resource conditions are held constant, these spatial patterns constitute the principal controlled difference among the three scenarios. Figure 6b shows the corresponding model-derived local conflict-intensity distributions. The clustered configuration produces concentrated interaction regions associated with locally concentrated demand, whereas the uniform configuration produces a more spatially dispersed conflict pattern. The crossing configuration generates localized interaction regions around intersecting traffic flows. Thus, the comparison should be interpreted as a controlled assessment of how different traffic organization redistributes local operational pressure under otherwise identical demand and resource conditions, rather than as a comparison of three independently observed operational cases.

The quantitative comparison further confirms this observation. As shown in Figure 7, the three scenarios occupy different positions in the overload–extent space, demonstrating that identical resource availability does not guarantee equivalent operational feasibility. The clustered pattern exhibits higher local overload due to concentrated demand, while the crossing pattern produces localized interaction pressure around intersecting traffic flows. In contrast, the uniform pattern maintains relatively lower local resource pressure through spatial dispersion of demand.

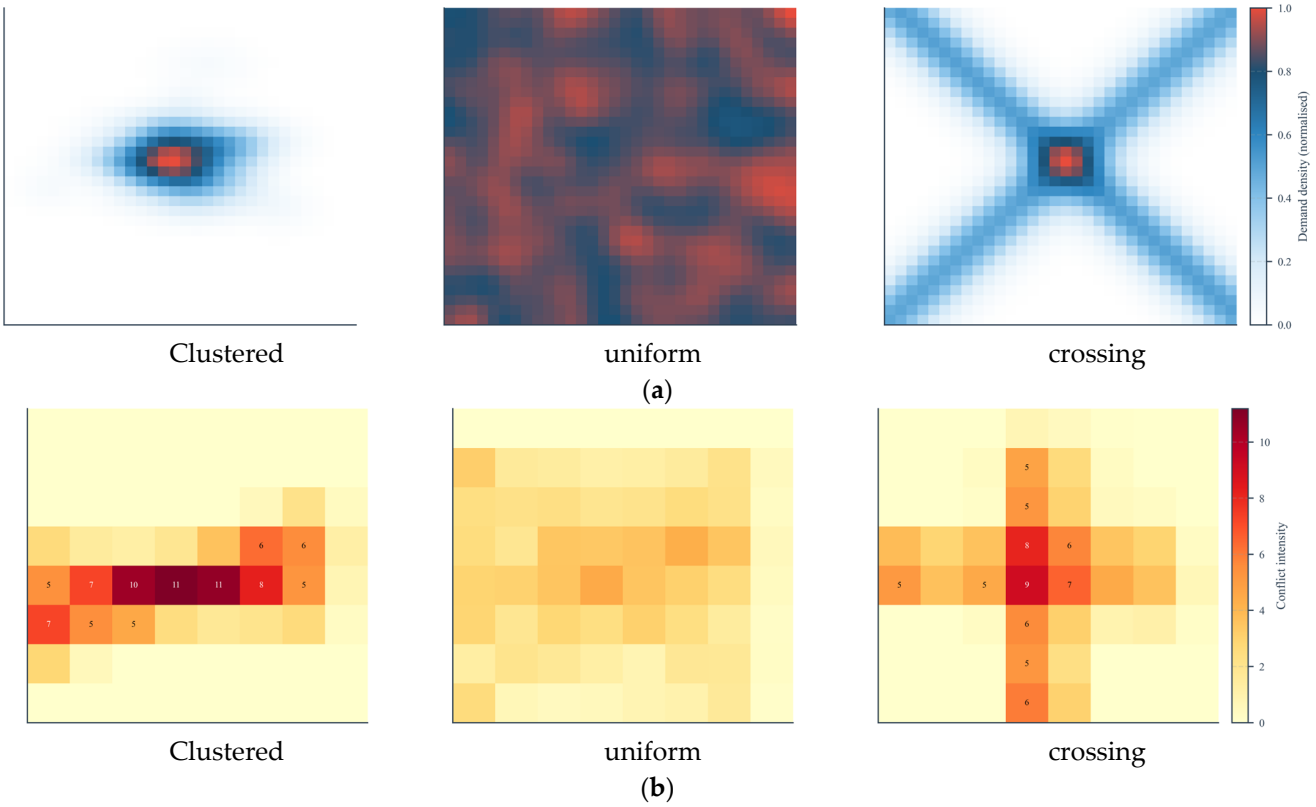


Figure 6. Controlled comparison of traffic spatial organization under identical resource and total-demand conditions: (**a**) constructed clustered, uniform, and crossing traffic configurations; and (**b**) corresponding model-derived local interaction-intensity distributions.

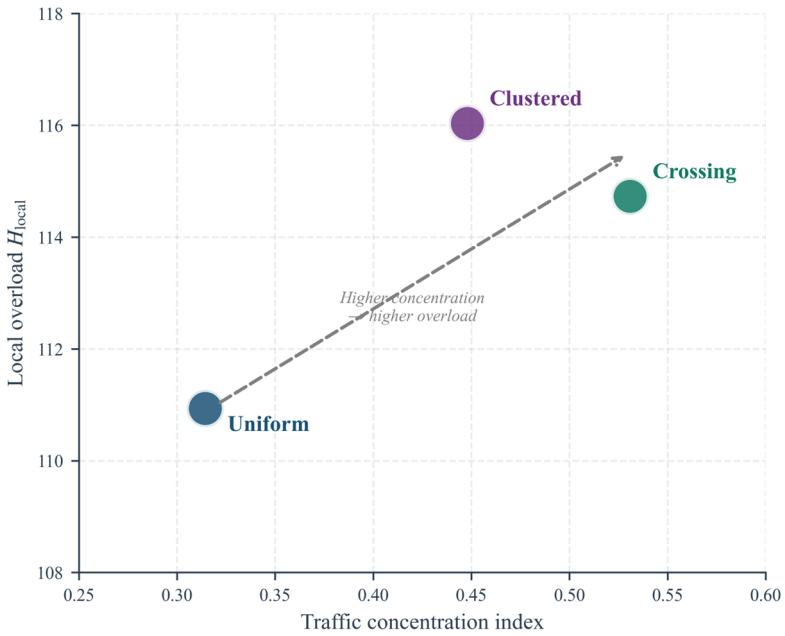


Figure 7. Relationship between local overload and active-region overload proportion under the three traffic-organization scenarios.

These results demonstrate that terminal airspace capacity is not only determined by the amount of available resources but also by the spatial organization of traffic demand. Therefore, accurate dynamic capacity assessment requires consideration of both resource availability and traffic-resource interaction mechanisms. The proposed SRE framework

captures these localized effects by maintaining the correspondence between traffic demand and available operational resources.

5.5. Robustness Analysis

5.5.1. Sensitivity to Discretization and Model Parameters

To assess whether the principal SRE-based findings depend strongly on the adopted discretization or model parameters, the sensitivity tests described in Section 4.4.2 were performed. The ordering of the four weather scenarios remained Clear > Mild > Moderate > Severe under all tested configurations, and the matched–mismatched local-overload difference remained positive in every case. These results indicate that the resource-degradation and spatial-mismatch mechanisms are qualitatively robust to the tested modelling choices. The sensitivity test results are summarized in Table 4.

Table 4. Sensitivity of the principal SRE-based indicators to discretization and parameter settings.

Configuration	I_{sup}^{Clear}	$\Delta H_{Moderate}$(*SRE-eq*)
Baseline	0.743	13.45
Grid 20 × 20	0.727	11.28
Grid 40 × 40	0.707	14.91
Δt = 2.5 min	0.743	12.55
Δt = 10 min	0.743	11.71
w = [0.6, 0.2, 0.2]	0.762	13.53
w = [0.2, 0.6, 0.2]	0.772	15.38
w = [0.2, 0.2, 0.6]	0.695	12.28
Thresholds −20%	0.743	4.27
Thresholds +20%	0.653	25.24

The normalized clear-weather resource-capacity index I_{sup}^{Clear} varied from 0.653 to 0.772 across the tested settings, whereas the local-overload difference ΔH ranged from 4.27 to 25.24 SRE-eq. Variations in grid resolution, time step, and supply-weight allocation produced moderate quantitative changes without altering the qualitative scenario ordering or the sign of ΔH. In contrast, perturbation of the feasibility thresholds produced the largest change in ΔH, indicating that the magnitude of local overload is particularly sensitive to the adopted gating thresholds. Overall, the mechanism-level conclusions remain stable, while absolute overload magnitude should be interpreted with reference to the specified parameter configuration. Overall, although the numerical values of the SRE-derived indicators varied with discretization and parameter settings, the relative ordering of the weather scenarios and the identified resource-degradation and spatial-mismatch mechanisms remained stable across all tested grid resolutions, time steps, supply-weight sets, and gate-threshold perturbations. This suggests that the principal mechanism-level conclusions are robust, while the absolute magnitude of local overload should be interpreted with reference to the adopted threshold configuration.

5.5.2. Robustness Across Additional Operating Periods

To examine whether the mechanism-level findings obtained from the baseline case were specific to a single three-hour traffic sample, an additional cross-period robustness assessment was conducted using three operating periods with different observed traffic levels. Daily ADS-B archives were screened using a predefined procedure over the fixed 12:00–15:00 UTC window within the EHAM study domain. Among the available archives, the valid periods were ranked according to the number of active airborne aircraft, and representative low-, median-, and high-traffic periods were selected. The resulting periods contained 110 aircraft on 25 September 2024, 250 aircraft on 23 December 2024, and 341

aircraft on 27 October 2024, respectively. The same study domain, SRE discretization, model parameters, weather-degradation settings, and matched/mismatched scenario definitions were applied to all three periods.

As summarized in Table 5, the principal mechanism-level relationships remained consistent across the three traffic conditions. Under the same severe-weather resource-degradation setting, the normalized resource-capacity index decreased by 27.8% relative to the clear-weather baseline in all three periods. Under the spatial-mismatch experiment, the local overload H_{local} increased from 10.44 to 14.00 in the low-traffic period, from 27.09 to 31.81 in the median-traffic period, and from 38.78 to 43.60 in the high-traffic period. The corresponding relative increases were 34.0%, 17.4%, and 12.5%, respectively.

Table 5. Cross-period robustness under different traffic conditions.

Traffic Condition	Active Aircraft	Severe-Weather Change in I_{sup}	Matched Time-Averaged H_{local}	Mismatched Time-Averaged H_{local}	Relative Mismatch Increase
Low	110	−27.8%	10.44	14.00	+34.0%
Median	250	−27.8%	27.09	31.81	+17.4%
High	341	−27.8%	38.78	43.60	+12.5%

Although the absolute level of local overload increased with traffic demand, spatial mismatch consistently produced a higher H_{local} than the matched condition. These cross-period results indicate that the identified resource-degradation and spatial-mismatch relationships are not restricted to the original traffic sample, but remain qualitatively stable across substantially different traffic backgrounds within the same terminal area.

6. Conclusions

This study developed a spatio-temporal resource element (SRE)-based framework for mechanism-oriented assessment of dynamic terminal airspace capacity. The framework represents physical airspace availability, meteorological conditions, and surveillance support on the resource-supply side and maps aircraft operations onto task demand at the same spatio-temporal scale. Its principal methodological feature is that resource supply and task demand are matched locally before spatial aggregation, thereby preserving spatial correspondence and preventing resource surpluses in unconstrained regions from masking localized shortages.

The controlled case-study experiments reveal three complementary mechanisms. First, under fixed traffic demand, weather-induced resource degradation reduces the normalized SRE resource-capacity state while conventional demand-oriented indicators remain unchanged. Second, under identical global supply and demand, spatial mismatch produces greater local overload than a spatially matched configuration, confirming that global resource equivalence does not imply equivalent local operational feasibility. Third, different traffic organization generates distinct local interaction patterns even when total aircraft demand and resource conditions are held constant.

An SRE-independent aircraft-level trajectory benchmark was additionally introduced to examine the operational interpretation of SRE-derived local overload. Under the primary 3 NM/1000 ft separation criterion, median separation-constrained feasible throughput increased from 44 aircraft at a candidate demand of 50 to 207 aircraft at a candidate demand of 350, while the feasible acceptance ratio decreased from 0.88 to 0.59. No saturation plateau was observed within the tested demand range. After controlling for candidate demand, cumulative SRE local overload remained positively associated with independently rejected demand $\rho = 0.452$, $p = 4.9 \times 10^{-19}$; the association was also robust to alternative trajectory-resampling intervals. These findings provide an independent trajectory-based operational-feasibility reference for the SRE diagnostics without relying on an SRE-defined throughput threshold.

The principal mechanism-level findings were furthermore stable under alternative spatial grids, temporal resolutions, supply-weight allocations, and feasibility thresholds. Cross-period tests using low-, median-, and high-traffic operating windows also reproduced both the resource-degradation and spatial-mismatch relationships, indicating that the identified mechanisms are not restricted to the original three-hour traffic sample.

Several limitations remain. The independent trajectory benchmark is separation-constrained and operates on fixed observed trajectories; it therefore should not be interpreted as an independently observed ATC capacity value. Controller interventions, rerouting, delay assignment, altitude changes, and conflict-resolution manoeuvres are not represented. The empirical evaluation is also limited to a single terminal area, while the weather-degradation, spatial-mismatch, and traffic-organization experiments are controlled, parameterized scenarios rather than independently observed capacity-restriction events. In addition, absolute SRE-eq values depend on the selected spatial and temporal discretization and on model parameters such as feasibility thresholds and resource-supply weights. Future work should therefore extend the framework to multiple terminal areas and longer operational periods, incorporate independently observed throughput restrictions, delays, and controller-workload measurements, and couple SRE diagnostics with trajectory optimization and controller-response models to support closed-loop operational evaluation.

Author Contributions: Conceptualization, D.H. and D.S.; methodology, D.H.; software, D.H.; validation, D.H., D.S. and F.Y.; formal analysis, D.H.; investigation, D.H.; resources, D.S.; data curation, D.H.; writing—original draft preparation, D.H.; writing—review and editing, D.S., F.Y., X.Z. and J.T.; visualization, D.H.; supervision, D.S.; project administration, D.S. All authors have read and agreed to the published version of the manuscript.

Funding: This research received no external funding.

Data Availability Statement: The ADS-B trajectory data used in this study were obtained from the OpenSky Network. Meteorological data were obtained from Open-Meteo records. The processed datasets and simulation results generated during this study are available from the corresponding author upon reasonable request.

Acknowledgments: The authors would like to thank the OpenSky Network for providing publicly available ADS-B trajectory data and Open-Meteo for providing the meteorological information used in this study.

Conflicts of Interest: The authors declare no conflicts of interest.

Abbreviations

The following abbreviations are used in this manuscript:

SRE	Spatio-Temporal Resource Element
ATM	Air Traffic Management
DCB	Demand–Capacity Balancing
EHAM	Amsterdam Airport Schiphol (ICAO airport code)
ADS-B	Automatic Dependent Surveillance–Broadcast
SRE-eq	Spatio-Temporal Resource Element Equivalent

References

1. International Civil Aviation Organization (ICAO). *Global Air Traffic Management Operational Concept*; ICAO Doc 9854; International Civil Aviation Organization: Montreal, QC, Canada, 2005.
2. European Organisation for the Safety of Air Navigation (EUROCONTROL). *Capacity Assessment and Planning Guidance Document*; EUROCONTROL: Brussels, Belgium, 2013.
3. Gilbo, E.P. Airport Capacity: Representation, Estimation, Optimization. *IEEE Trans. Control Syst. Technol.* **1993**, *1*, 144–154. [CrossRef] [PubMed]

4. Janić, M.; Tošić, V. Terminal Airspace Capacity Model. *Transp. Res. Part A Gen.* **1982**, *16*, 253–260. [CrossRef]
5. Gilbo, E.P. Optimizing Airport Capacity Utilization in Air Traffic Flow Management Subject to Constraints at Arrival and Departure Fixes. *IEEE Trans. Control Syst. Technol.* **1997**, *5*, 490–503. [CrossRef]
6. Lee, H.; Feron, E.; Pritchett, A. Air Traffic Complexity and the Controller: Preliminary Results. In *AIAA Guidance, Navigation, and Control Conference*; AIAA: Reston, VA, USA, 2007.
7. Laudeman, I.V.; Shelden, S.G.; Branstrom, R.; Brasil, C.L. *Dynamic Density: An Air Traffic Management Metric*; NASA Technical Memorandum NASA/TM-1998-112226; NASA Ames Research Center: Moffett Field, CA, USA, 1998.
8. Sridhar, B.; Sheth, K.; Grabbe, S. Airspace Complexity and Its Application in Air Traffic Management. In Proceedings of the 2nd USA/Europe Air Traffic Management R&D Seminar, Orlando, FL, USA, 1–4 December 1998.
9. Netjasov, F.; Janić, M.; Tošić, V. Developing a Generic Metric of Terminal Airspace Traffic Complexity. *Transportmetrica* **2011**, *7*, 369–394. [CrossRef]
10. Yang, W.; Garcia-Rivera, J.M.; Petty, M.A.; Layne, G.J.; Fenton, K.; Cheng, J.; Chen, R.; Guo, W.; Weng, Y.; Liu, S.; et al. Quantifying Convective Weather Impacts to Airspace Capacity: Framework and Preliminary Results. *J. Air Transp.* **2021**, *29*, 42–55. [CrossRef]
11. SESAR Joint Undertaking. *European ATM Master Plan: Digitalising Europe's Aviation Infrastructure*; SESAR Joint Undertaking: Brussels, Belgium, 2019.
12. Gardi, A.; Sabatini, R.; Kistan, T. Four-Dimensional Trajectory Management in Air Traffic Control: A Review of Emerging Technologies and Operational Concepts. *IEEE Trans. Aerosp. Electron. Syst.* **2018**, *54*, 1185–1202.
13. Delgado, L.; Prats, X. Effect of Weather Uncertainty on Air Traffic Management Performance. *Transp. Res. Part C Emerg. Technol.* **2013**, *33*, 107–120.
14. Jacquillat, A.; Odoni, A.R. A Scalable Approach to Dynamic Air Traffic Flow Management under Capacity Uncertainty. *Transp. Res. Part C Emerg. Technol.* **2015**, *63*, 207–223.
15. Pyrgiotis, N.; Malone, K.M.; Odoni, A. Modelling Delay Propagation within an Airport Network. *Transp. Res. Part C Emerg. Technol.* **2013**, *27*, 60–75. [CrossRef]
16. Bertsimas, D.; Lulli, G.; Odoni, A. An Integer Optimization Approach to Large-Scale Air Traffic Flow Management. *Oper. Res.* **2011**, *59*, 211–227. [CrossRef]
17. Prandini, M.; Piroddi, L.; Puechmorel, S.; Brázdilová, L. Toward Air Traffic Complexity Assessment in New Generation Air Traffic Management Systems. *IEEE Trans. Intell. Transp. Syst.* **2011**, *12*, 809–818. [CrossRef]
18. Brázdilová, S.L.; Císek, P.; Kubalčík, J. Air Traffic Complexity for a Distributed Air Traffic Management System. *Proc. Inst. Mech. Eng. Part G J. Aerosp. Eng.* **2011**, *225*, 875–886. [CrossRef]
19. Majumdar, A.; Ochieng, W.Y. Factors Affecting Air Traffic Controller Workload: Multivariate Analysis Approach. *Transp. Res. Rec.* **2002**, *1788*, 58–69. [CrossRef]
20. Gariel, M.; Srivastava, A.N.; Feron, E. Trajectory Clustering and an Application to Air Traffic Analysis. *IEEE Trans. Intell. Transp. Syst.* **2011**, *12*, 663–674. [CrossRef]
21. Chatterji, G.B.; Sridhar, B. Measures for Air Traffic Complexity. In Proceedings of the AIAA Guidance, Navigation, and Control Conference, Monterey, CA, USA, 5–8 August 2002.
22. Odoni, A.R. The Flow Management Problem in Air Traffic Control. In *Flow Control of Congested Networks*; Springer: Berlin, Germany, 1987; pp. 293–303.
23. Mas-Pujol, S.; Salamí, E.; Pastor, E. Image-Based Multi-Agent Reinforcement Learning for Demand–Capacity Balancing. *Aerospace* **2022**, *9*, 599. [CrossRef]
24. Kravaris, T.; Lentzos, K.; Santipantakis, G.; Vouros, G.A.; Andrienko, G.; Andrienko, N.; Crook, I.; Garcia, J.M.C.; Martinez, E.I. Explaining Deep Reinforcement Learning Decisions in Complex Multiagent Settings: Towards Enabling Automation in Air Traffic Flow Management. *Appl. Intell.* **2023**, *53*, 4063–4098. [CrossRef] [PubMed]
25. Chen, Y.; Xu, Y.; Hu, M. General Multi-Agent Reinforcement Learning Integrating Heuristic-Based Delay Priority Strategy for Demand and Capacity Balancing. *Transp. Res. Part C Emerg. Technol.* **2023**, *153*, 104218. [CrossRef]

Disclaimer/Publisher's Note: The statements, opinions and data contained in all publications are solely those of the individual author(s) and contributor(s) and not of MDPI and/or the editor(s). MDPI and/or the editor(s) disclaim responsibility for any injury to people or property resulting from any ideas, methods, instructions or products referred to in the content.